Available online at www.sciencedirect.com
SCIENCE DIRECT®
Journal of Sound and Vibration 283 (2005) 723–748
JOURNAL OF SOUND AND VIBRATION
www.elsevier.com/locate/jsvi

The mapping dynamics of periodic motions for a three-piecewise linear system under a periodic excitation

Albert C.J. Luo*

Department of Mechanical and Industrial Engineering, Southern Illinois University Edwardsville, Edwardsville, IL 62026-1805, USA

Received 1 August 2003; accepted 11 May 2004
Available online 11 November 2004

Abstract

In this paper, the mapping dynamics of periodic motions for a three-piecewise linear system under a periodic excitation is developed, and the mapping structures for specified periodic motions are constructed. Based on the mapping structures, an analytical prediction of all possible, stable and unstable periodic motions is given. The symmetry for the stable, asymmetrical, periodic motions of such a system is observed. However, the unstable periodic motions do not have such symmetry. The methodology presented in this paper is applicable to other non-smooth systems such as friction-induced vibration, impact oscillator and power control systems. In addition, the mapping dynamics provides a useful and efficient tool for the co-existence of periodic motions and/or chaotic motions in nonlinear dynamical systems.

1. Introduction

The mapping dynamics of periodic motions for any dynamical system is to develop the mapping relationships from which the expected periodic motions can be analytically predicted. This investigation will avoid passive digital simulations of dynamics responses in nonlinear dynamical systems, and also this investigation will provide a possibility to obtain all stable and

*Tel.: +1-618-650-5389; fax: +1-618-650-2555.
E-mail address: aluo@siue.edu (A.C.J. Luo).

0022-460X/$ - see front matter © 2004 Elsevier Ltd. All rights reserved.
doi:10.1016/j.jsv.2004.05.023

unstable periodic motions existing in dynamical systems rather than only one of stable motions given by numerical simulations. The mapping dynamics herein will provide a useful and efficient tool for us to determine the co-existence of periodic motions and/or chaos. The mapping has been extensively used for investigation of complicated motions in nonlinear systems since Poincaré [1] introduced the mapping concept for determination of periodic responses in nonlinear dynamics. Such a mapping is termed the Poincaré mapping. The mapping sets accompanying the Poincaré mapping is termed the Poincaré mapping section or surface. For an N-dimensional autonomous system, the Poincaré mapping section is selected as an $(N-1)$-dimensional surface transversal to the closed orbit. When a periodically driven, N-dimensional *continuous* system is investigated, the Poincaré mapping section is often constructed by an N-dimensional set of responses in phase space. However, for a periodically driven, N-dimensional *discontinuous* system, discontinuous surfaces are a candidate of the Poincaré mapping section. In beginning of the last century, one used the Poincaré mapping method for periodic motion and stability [2,3]. Since the middle of last century, the Poincaré mapping has been used to demonstrate chaotic motions (e.g., Refs. [4,5]).

In 1983, Shaw and Holmes [6] investigated a piecewise linear system with a single discontinuity through the Poincaré mapping and numerically predicted chaotic motion. In 1991, Nordmark [7] used the mapping technique to investigate non-periodic motion caused by the grazing bifurcation. In 1992 Kleczka et al. [8] investigated the periodic motion and bifurcations of piecewise linear oscillator motion, and numerically observed the grazing motion. Foale [9] used Nordmark's idea about the grazing bifurcation to analytically determine the bifurcation in the impact oscillator in 1994. To determine complex periodic motions, in 1995 Luo [10] initialized the concept of mapping dynamics for discontinuous systems and applied it to impacting oscillators and a ball bouncing on a vibrating table (also see Refs. [11,12]). In 2002, Luo [13] discovered the two asymmetric period-1 motions by introduction of a time interval between two impacts, and one of the two asymmetric motions for such an impact system were observed through a numerical investigation in Ref. [14]. In 2003, Menon and Luo [15] used the concept of mapping dynamics to construct mapping structures of a piecewise linear system with a dead-zone restoring force. In addition, without the mapping techniques, the following contributions to the piecewise linear system problem should be mentioned. The early study of a piecewise linear system without damping was completed by Hartog and Mikina [16] in 1932 and a closed-form solution for symmetric and periodic motion was obtained. Timoshenko [17] discussed undamped piecewise linear systems in 1937. In 1989, Natsiavas [18] identified the responses of a system with tri-linear springs with a time-incremental method, and by use of a similar approach, the dynamics of oscillators with strongly nonlinear asymmetric damping was investigated [19]. In 2000, Theodossiades and Natsiavas [20] discussed the modeling of gear-pair vibration as a piecewise linear problem, and the periodic solutions and stability for such a system were discussed.

In this paper, the mapping dynamics of periodic motion will be investigated for a better understanding of the complex periodic motions in a three-piecewise linear system under a periodic excitation, and mapping structures for specified periodic motions will be developed. An analytical prediction of all possible, stable and unstable periodic motions will be given from those mapping structures. The local stability and bifurcation will be obtained through eigenvalue analysis. Numerical simulations are presented for demonstration of the symmetry of periodic motions.

2. Switching sets and generic mappings

Consider a periodically excited, piecewise linear system

$$\ddot{x} + 2d\dot{x} + k(x) = a\cos\Omega t, \tag{1}$$

where $\dot{x} = \mathrm{d}x/\mathrm{d}t$. The parameters Ω and a are excitation frequency and amplitude, respectively. The restoring force is

$$k(x) = \begin{cases} cx - e & \text{for } x \geqslant E, \\ 0 & \text{for } -E \leqslant x \leqslant E, \\ cx + e & \text{for } x \leqslant -E, \end{cases} \tag{2}$$

with $E = e/c$. In the foregoing system, there are three linear regions of the restoring force (Region I: $x \geqslant E$, Region II: $-E \leqslant x \leqslant E$ and Region III: $x \leqslant -E$). The solution for each region can be easily obtained, as listed in Appendix A.

For description of motion in Eq. (1), two switching sections (or sets) are defined as

$$\Sigma^+ = \{(t_i, x_i, y_i) | x_i = E, \dot{x}_i = y_i\} \quad \text{and} \quad \Sigma^- = \{(t_i, x_i, y_i) | x_i = -E, \dot{x}_i = y_i\}. \tag{3}$$

The two sets are decomposed into

$$\Sigma^+ = \Sigma^+_+ \cup \Sigma^+_- \cup \{t_i, E, 0\} \quad \text{and} \quad \Sigma^- = \Sigma^-_+ \cup \Sigma^-_- \cup \{t_i, -E, 0\}, \tag{4}$$

where four subsets are defined as

$$\Sigma^+_+ = \{(t_i, x_i, y_i) | x_i = E, \dot{x}_i = y_i > 0\} \quad \text{and} \quad \Sigma^+_- = \{(t_i, x_i, y_i) | x_i = E, \dot{x}_i = y_i < 0\}, \tag{5}$$

$$\Sigma^-_+ = \{(t_i, x_i, y_i) | x_i = -E, \dot{x}_i = y_i > 0\} \quad \text{and} \quad \Sigma^-_- = \{(t_i, x_i, y_i) | x_i = -E, \dot{x}_i = y_i < 0\}. \tag{6}$$

The points $\{t_i, E, 0\}$ and $\{t_i, -E, 0\}$ strongly dependent on the external force direction are singular. From four subsets, six basic mappings are

$$\begin{aligned} &P_1 : \Sigma^+_+ \to \Sigma^+_-, \quad P_2 : \Sigma^+_- \to \Sigma^-_-, \quad P_3 : \Sigma^-_- \to \Sigma^-_+, \\ &P_4 : \Sigma^-_+ \to \Sigma^+_+, \quad P_5 : \Sigma^+_- \to \Sigma^+_+, \quad P_6 : \Sigma^-_+ \to \Sigma^-_-. \end{aligned} \tag{7}$$

In Fig. 1, the switching planes and basic mappings are sketched. The mapping $P_1 : (t_i, E, y_i) \to (t_{i+1}, E, y_{i+1})$ indicates that the initial and final states are $(t, x, \dot{x})_{\text{initial}} = (t_i, E, y_i)$ and $(t, x, \dot{x})_{\text{final}} = (t_{i+1}, E, y_{i+1})$ in Region I, respectively. For $y_i > 0$ and $y_{i+1} < 0$, two governing equations for mapping P_1 are obtained from Eqs. (A.2) and (A.3) with $x_i = E$, i.e.,

$$\begin{aligned} &[C_1(t_i)\cos\omega(t_{i+1} - t_i) + C_2(t_i, y_i)\sin\omega(t_{i+1} - t_i)]\mathrm{e}^{-d(t_{i+1}-t_i)} + a(D_1\cos\Omega t_{i+1} + D_2\sin\Omega t_{i+1}) = 0, \\ &y_{i+1} + \{[C_1(t_i)d - C_2(t_i, y_i)\omega]\cos\omega(t_{i+1} - t_i) + [C_1(t_i)\omega + C_2(t_i, y_i)d]\sin\omega(t_{i+1} - t_i)\}\mathrm{e}^{-d(t_{i+1}-t_i)} \\ &\quad + a\Omega(D_1\sin\Omega t_{i+1} - D_2\cos\Omega t_{i+1}) = 0. \end{aligned} \tag{8}$$

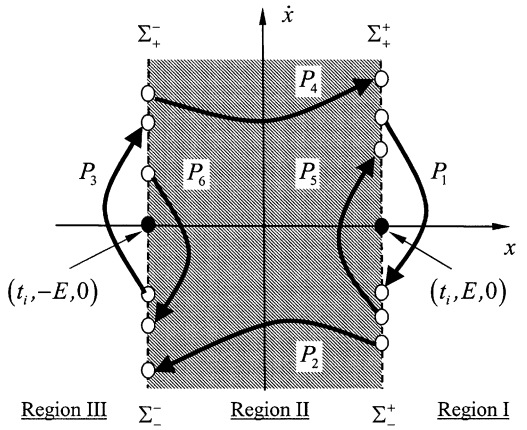

Fig. 1. Switching sections and generic mappings in phase plane.

Similarly, the mapping $P_2 : (t_i, E, y_i) \to (t_{i+1}, -E, y_{i+1})$ gives the initial and final states (t_i, E, y_i) and $(t_{i+1}, -E, y_{i+1})$ in Region II, respectively. The corresponding governing equations for the mapping P_2 are obtained from Eqs. (A.7) and (A.8) plus $x_i = E$ for $y_i < 0$ and $y_{i+1} < 0$, i.e.,

$$\begin{aligned} &C_3(t_i, y_i)\mathrm{e}^{-2d(t_{i+1}-t_i)} + C_4(t_i, y_i) + a(D_3 \cos \Omega t_{i+1} + D_4 \sin \Omega t_{i+1}) + 2E = 0,\\ &y_{i+1} + 2dC_3(t_i, y_i)\mathrm{e}^{-2d(t_{i+1}-t_i)} + a\Omega(D_3 \sin \Omega t_{i+1} - D_4 \cos \Omega t_{i+1}) = 0. \end{aligned} \tag{9}$$

The motion of the system enters Region III after time t_i, and returns back to the boundary of Regions II and III until time t_{i+1}. Such a motion is measured through the mapping P_3. Note that for $y_i < 0$ and $y_{i+1} > 0$, Eqs. (A.2) and (A.3) with $x_i = -E$ give the governing equations as in Eq. (8).

The mapping P_4 brings the motion from the boundary of Regions III and II at time t_i to the boundary of Regions II and I at time t_{i+1}. The governing equations for such a mapping are determined by Eqs. (A.7) and (A.8) with $(t_i, -E, y_i)$ and (t_{i+1}, E, y_{i+1}) for $y_i > 0$ and $y_{i+1} > 0$, i.e.,

$$\begin{aligned} &C_3(t_i, y_i)\mathrm{e}^{-2d(t_{i+1}-t_i)} + C_4(t_i, y_i) + a(D_3 \cos \Omega t_{i+1} + D_4 \sin \Omega t_{i+1}) - 2E = 0,\\ &y_{i+1} + 2dC_3(t_i, y_i)\mathrm{e}^{-2d(t_{i+1}-t_i)} + a\Omega(D_3 \sin \Omega t_{i+1} - D_4 \cos \Omega t_{i+1}) = 0. \end{aligned} \tag{10}$$

The mapping P_5 brings the motion from the boundary of Regions I and II to the boundary of Regions I and II at time t_{i+1}. The governing equations for such a mapping are determined by Eqs. (A.7) and (A.8) with (t_i, E, y_i) and (t_{i+1}, E, y_{i+1}) for $y_i < 0$ and $y_{i+1} > 0$, i.e.,

$$\begin{aligned} &C_3(t_i, y_i)\mathrm{e}^{-2d(t_{i+1}-t_i)} + C_4(t_i, y_i) + a(D_3 \cos \Omega t_{i+1} + D_4 \sin \Omega t_{i+1}) = 0,\\ &y_{i+1} + 2dC_3(t_i, y_i)\mathrm{e}^{-2d(t_{i+1}-t_i)} + a\Omega(D_3 \sin \Omega t_{i+1} - D_4 \cos \Omega t_{i+1}) = 0. \end{aligned} \tag{11}$$

The mapping P_6 maps the motion from the boundary of Regions II and III to the boundary of Regions II and III at time t_{i+1}. The governing equations for such a mapping are the same as in Eq. (11) with $y_i > 0$ and $y_{i+1} < 0$. From the above mapping definitions, mappings P_1, P_3, P_5 and P_6 are termed the local mapping, and mappings P_2 and P_4 are termed the global mapping (or the transfer mapping).

3. Mapping structures

For simplicity, the following notation for mapping is introduced:

$$P_{n_1 n_2 \cdots n_k} \equiv P_{n_1} \circ P_{n_2} \circ \cdots \circ P_{n_k}, \tag{12}$$

where $P_{n_i} \in \{P_j | j = 1, 2, \ldots, 6\}$ and $n_i = \{1, 2, \ldots, 6\}$. Note that the rotation of the mapping of periodic motion in order gives the same motion (i.e., $P_{n_1 n_2 \cdots n_k}, P_{n_2 \cdots n_k n_1}, \ldots, P_{n_k n_1 \cdots n_{k-1}}$), and only the selected Poincaré mapping section is different. The motion of the *m-time* repeating of mapping $P_{n_1 n_2 \cdots n_k}$ is defined as

$$\begin{aligned} P^m_{n_1 n_2 \cdots n_k} &\equiv P_{(n_1 n_2 \cdots n_k)^m} \equiv P_{\underbrace{(n_1 n_2 \cdots n_k) \cdots (n_1 n_2 \cdots n_k)}_{m}} \\ &\equiv \underbrace{(P_{n_1} \circ P_{n_2} \circ \cdots \circ P_{n_k}) \circ \cdots \circ (P_{n_1} \circ P_{n_2} \circ \cdots \circ P_{n_k})}_{m\text{-sets}}. \end{aligned} \tag{13}$$

To extend this concept to the local mapping, define

$$P^m_{15} \equiv P_{(15)^m} \equiv \underbrace{(P_1 \circ P_5) \circ \cdots \circ (P_1 \circ P_5)}_{m\text{-sets}} \quad \text{and} \quad P^m_{36} \equiv P_{(36)^m} \equiv \underbrace{(P_3 \circ P_6) \circ \cdots \circ (P_3 \circ P_6)}_{m\text{-sets}}. \tag{14}$$

For the special combination of global and local mapping, introduce a mapping structure

$$\begin{aligned} P_{n_1 n_2 \cdots (n_i n_l)^m \cdots n_k} &\equiv P_{n_1} \circ P_{n_2} \circ \cdots \circ P^m_{n_i n_l} \circ \cdots \circ P_{n_k} \\ &= P_{n_1} \circ P_{n_2} \circ \cdots \circ \underbrace{(P_{n_i} \circ P_{n_l}) \circ \cdots \circ (P_{n_i} \circ P_{n_l})}_{m\text{-sets}} \circ \cdots \circ P_{n_k}. \end{aligned} \tag{15}$$

From the definition, the motion of Eq. (1) can be very easily labeled through the mapping structure accordingly.

3.1. Local periodic motion

Since there are two displacement constraints, there are many possible periodic motion models. Consider local periodic motions near two displacement constraints first, namely, no transfer mapping is used to map the switching planes from one to another. To construct the Poincaré mapping for the motion from Σ^+_+ to Σ^+_+, the commutative diagram for period-1 and period-k motion is illustrated in Figs. 2(a) and (b), respectively. The corresponding physical motions near the displacement constraint at $x = E$ are presented in Figs. 2(c) and (d). From the mapping commutative diagram, the period-1 and period-k motions possess the Poincaré mapping $P : \Sigma^+_+ \to \Sigma^+_+$ with the following mapping relations:

$$P_{51} = P_5 \circ P_1 \quad \text{and} \quad P^k_{51} \equiv P_{\underbrace{(51) \cdots (51)}_{k}} = \underbrace{(\underbrace{P_5 \circ P_1}_{\text{final pair}}) \circ \cdots \circ (\underbrace{P_5 \circ P_1}_{\text{initial pair}})}_{k\text{-pairs}}, \tag{16}$$

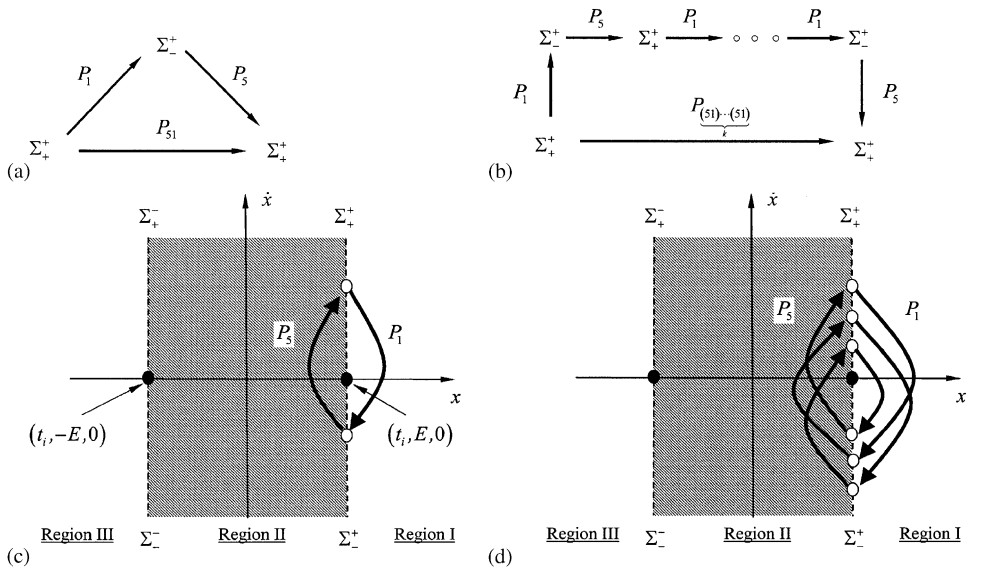

Fig. 2. Local periodic motion near the displacement at $x = E$: mapping commutative diagrams for (a) period-1 motion and (b) period-k motion; physical motion for (c) period-1 motion and (d) period-k motion.

where $P \equiv P_{51}$ and $P \equiv P_{51}^k$. Once the period-1 motion has period doubling, the integer k becomes 2. Therefore, the second equation in Eq. (16) includes all possible periodic motion for the different integer k. Similarly, if the switch plane Σ_-^+ is chosen as the Poincaré mapping section, the Poincaré mapping $P : \Sigma_-^+ \to \Sigma_-^+$ becomes

$$P_{15} = P_1 \circ P_5 \quad \text{and} \quad P_{15}^k \equiv P_{\underbrace{(15)\cdots(15)}_{k}} = \underbrace{\underbrace{(P_1 \circ P_5)}_{\text{final pair}} \circ \cdots \circ \underbrace{(P_1 \circ P_5)}_{\text{initial pair}}}_{k\text{-pairs}}. \tag{17}$$

In a similar manner, the Poincaré mapping for the periodic motion near the displacement constant $x = -E$ is defined as $P_{36} : \Sigma_-^- \to \Sigma_-^-$ or $P_{63} : \Sigma_-^- \to \Sigma_-^-$. For such a Poincaré mapping, the mapping commutative diagram and physical motion in phase planes are presented in Fig. 3. The Poincaré mapping is given by

$$P_{63} = P_6 \circ P_3 \quad \text{and} \quad P_{63}^k \equiv P_{\underbrace{(63)\cdots(63)}_{k}} = \underbrace{\underbrace{(P_6 \circ P_3)}_{\text{final pair}} \circ \cdots \circ \underbrace{(P_6 \circ P_3)}_{\text{initial pair}}}_{k-\text{pairs}}, \tag{18}$$

or

$$P_{36} = P_3 \circ P_6 \quad \text{and} \quad P_{36}^k \equiv P_{\underbrace{(36)\cdots(36)}_{k}} = \underbrace{\underbrace{(P_3 \circ P_6)}_{\text{final pair}} \circ \cdots \circ \underbrace{(P_3 \circ P_6)}_{\text{initial pair}}}_{k-\text{pairs}}. \tag{19}$$

The local periodic motion can be determined through these mapping relationships.

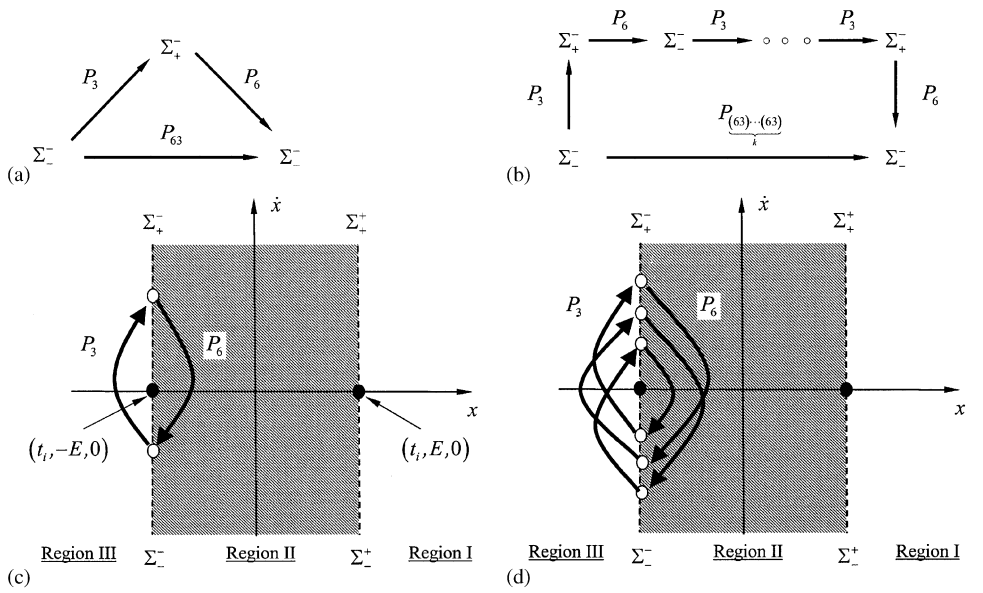

Fig. 3. Local periodic motion near the displacement at $x = -E$: mapping commutative diagrams for (a) period-1 motion and (b) period-k motion; physical motion for (c) period-1 motion and (d) period-k motion.

3.2. Global periodic motion

The global periodic motion is the motion that passes through the two displacement constraints. With varying system parameters, the motion described by P_5 and P_6 will convert to the motion determined by P_2 and P_4. The local periodic motion becomes a global motion through a grazing bifurcation or catastrophe with the Jacobian matrix singularity, and the global motion connects the two displacement constraints. Consider the simplest global periodic motion with a Poincaré mapping $P_{4321} : \Sigma_+^+ \to \Sigma_+^+$, and the mapping commutative diagram and physical model is given in Fig. 4. The Poincaré mapping is expressed by

$$P_{4321} = P_4 \circ P_3 \circ P_2 \circ P_1. \tag{20}$$

Once the period doubling of periodic motion in Eq. (20) occurs, the Poincaré mapping for period-2^k motion becomes

$$P_{4321}^{2^k} = \underbrace{\underbrace{P_4 \circ P_3 \circ P_2 \circ P_1}_{\text{final set}} \circ \cdots \circ \underbrace{P_4 \circ P_3 \circ P_2 \circ P_1}_{\text{initial set}}}_{2^k-\text{sets}}. \tag{21}$$

For the generalized Poincaré mapping for any period-k motion of mapping P_{4321}, we have

$$P_{4321}^{k} = \underbrace{\underbrace{P_4 \circ P_3 \circ P_2 \circ P_1}_{\text{final set}} \circ \cdots \circ \underbrace{P_4 \circ P_3 \circ P_2 \circ P_1}_{\text{initial set}}}_{k-\text{sets}}. \tag{22}$$

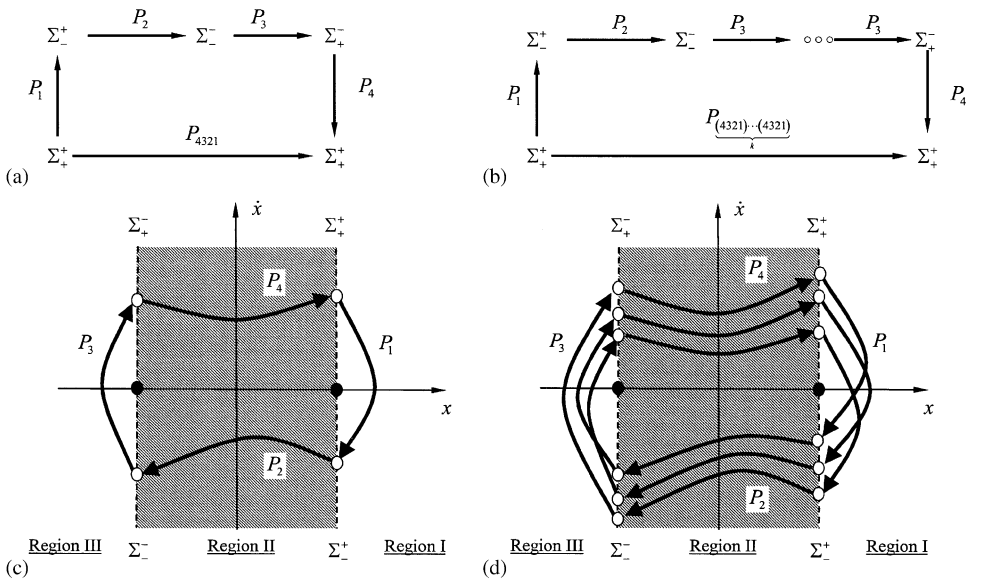

Fig. 4. The simplest global periodic motion: mapping commutative diagrams for (a) period-1 motion and (b) period-k motion; physical motion for (c) period-1 motion and (d) period-k motion.

3.3. Mixed periodic motion

The global periodic motion is not always symmetric, and with changing system parameters, the aforementioned local motions will be involved in the asymmetric, global motion to form a new periodic motion that is termed the mixed periodic motion. Therefore, the mixed periodic motion is combined with the local and global motions. Two basic models for such a mixed motion are presented through $P:\Sigma_+^+ \to \Sigma_+^+$, as shown in Fig. 5. The mapping structures for the simplest mixed periodic motion is expressed by

$$P_{432(15)1} = \underbrace{P_4 \circ P_3 \circ P_2 \circ \underbrace{P_1 \circ P_5}_{\text{local}} \circ P_1}_{\text{global}}, \quad \text{or} \quad P_{4(36)321} = \underbrace{P_4 \circ \underbrace{P_3 \circ P_6}_{\text{local}} \circ P_3 \circ P_2 \circ P_1}_{\text{global}}. \tag{23}$$

The two mixed motions are directly caused by the two different asymmetric motions of the global motion in Eq. (20). For the motion generated by the period-doubling bifurcation of mapping in Eq. (23), the mapping structures are the same as in Eq. (21). Namely, we have $P^{2^k}_{432(15)1} = P_{432(15)1} \circ \cdots \circ P_{432(15)1}$ and $P^{2^k}_{4(36)321} = P_{4(36)321} \circ \cdots \circ P_{4(36)321}$. Similarly, if the grazing or catastrophe with Jacobian matrix singularity exists, a new, mixed periodic motion will be generated from the two asymmetrical motions determined by mappings $P_{432(15)1}$ and $P_{4(36)321}$ in Eq. (23). The mapping structure of the new periodic motion is described by

$$P_{4(36)32(15)1} = P_4 \circ P_{36} \circ P_3 \circ P_2 \circ P_{15} \circ P_1 = \underbrace{P_4 \circ \underbrace{P_3 \circ P_6}_{\text{local}} \circ P_3 \circ P_2 \circ \underbrace{P_1 \circ P_5}_{\text{local}} \circ P_1}_{\text{global}}, \tag{24}$$

which is illustrated in Fig. 6.

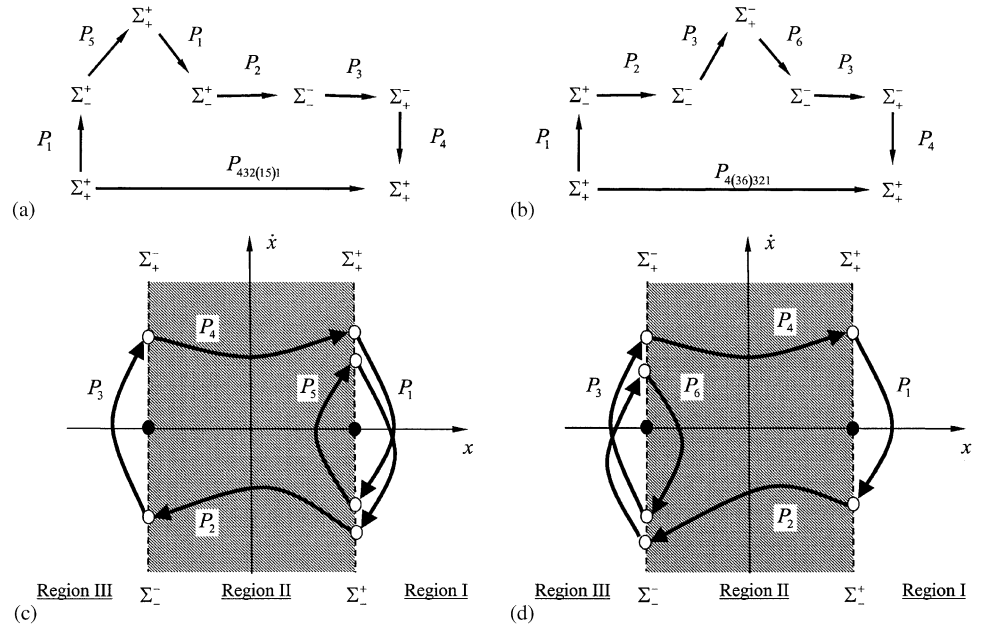

Fig. 5. The two asymmetric, global periodic motion: mapping commutative diagrams for (a) right- and (b) left-asymmetrical motions; physical motion for (c) right- and (d) left-asymmetrical motions.

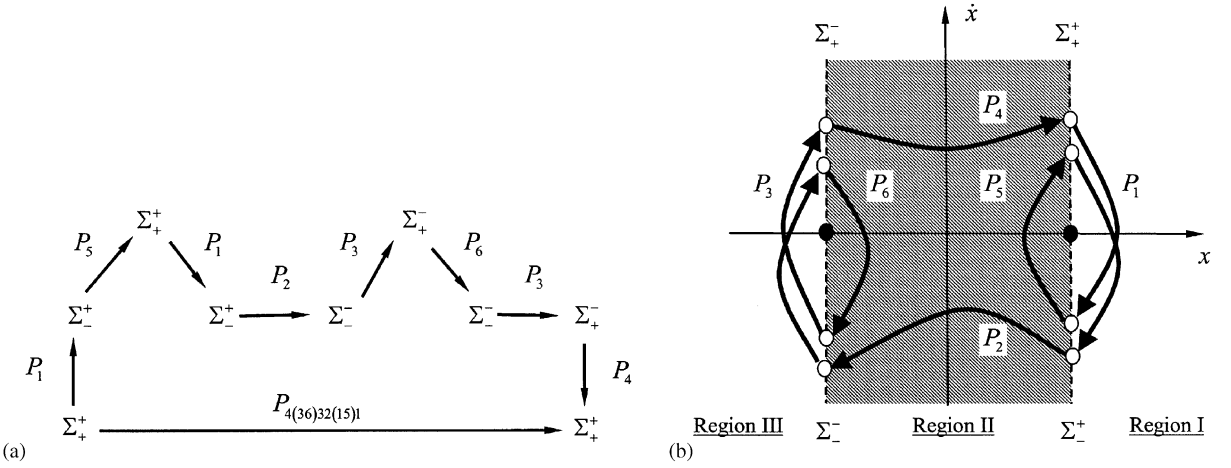

Fig. 6. The global periodic motion with two local cyclic motions: (a) mapping commutative diagram and (b) physical motion.

To generalize the above symmetrical and asymmetrical periodic motions, we have

$$\begin{aligned} P_{4(36)^{k_2}32(15)^{k_1}1} &= P_4 \circ P_{36}^{k_2} \circ P_3 \circ P_2 \circ P_{15}^{k_1} \circ P_1; \\ &= \underbrace{P_4 \circ \underbrace{P_3 \circ P_6 \circ \cdots \circ P_3 \circ P_6}_{k_2\text{-sct(local)}} \circ P_3 \circ P_2 \circ \underbrace{P_1 \circ P_5 \circ \cdots \circ P_1 \circ P_5}_{k_1\text{-sct(local)}} \circ P_1}_{\text{global}}. \end{aligned} \tag{25}$$

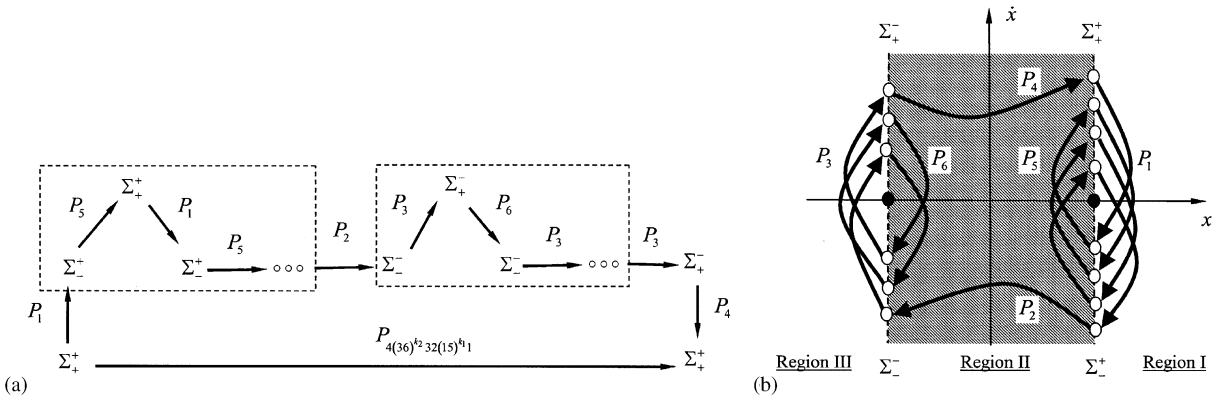

Fig. 7. A global periodic motion with k_2-cycle (left) and k_1-cycle (right) local motions: (a) mapping commutative diagram and (b) physical motion.

As $k_1 = k_2$, the foregoing mapping gives the motion possessing a symmetrical mapping. For $k_1 \neq k_2$, the motion having an asymmetrical mapping structure is obtained. The motion transition between the symmetrical and asymmetrical mappings, caused by grazing, will not be discussed herein, but the corresponding results will be presented in another paper. The mapping structure for Eq. (25) is presented in Fig. 7. The further generalized mapping structure for the complex, periodic motion is expressed by

$$
\begin{aligned}
&P_{4(36)^{k_{2n}}32(15)^{k_{1n}}1\cdots 4(36)^{k_{21}}32(15)^{k_{11}}1}\\
&\quad = P_4 \circ P_{36}^{k_{2n}} \circ P_3 \circ P_2 \circ P_{15}^{k_{1n}} \circ P_1 \circ \cdots \circ P_4 \circ P_{36}^{k_{21}} \circ P_3 \circ P_2 \circ P_{15}^{k_{11}} \circ P_1\\
&\quad = \underbrace{P_4 \circ \underbrace{P_3 \circ P_6 \circ \cdots \circ P_3 \circ P_6}_{k_{2n}\text{-set(local)}} \circ P_3 \circ P_2 \circ \underbrace{P_1 \circ P_5 \circ \cdots \circ P_1 \circ P_5}_{k_{1n}\text{-set(local)}} \circ P_1}_{n\text{-global}}\\
&\qquad \circ \cdots \circ \underbrace{P_4 \circ \underbrace{P_3 \circ P_6 \circ \cdots \circ P_3 \circ P_6}_{k_{21}\text{-set(local)}} \circ P_3 \circ P_2 \circ \underbrace{P_1 \circ P_5 \circ \cdots \circ P_1 \circ P_5}_{k_{11}\text{-set(local)}} \circ P_1}_{\text{first-global}} .
\end{aligned}
\tag{26}
$$

4. Stability and bifurcation

The periodic motion can be obtained through a specific Poincaré mapping given by one of the combined mappings developed in the previous section. In other words, the period-1 motion is determined by the fixed point of the Poincaré mapping for a given period $T = 2\pi/\Omega$ (i.e., mathematically, $P_{4(36)^{k_{2n}}32(15)^{k_{1n}}1\cdots 4(36)^{k_{21}}32(15)^{k_{11}}1}\mathbf{x}_i = \mathbf{x}_{i+4n+\sum_{m=1}^{n}(k_{2m}+k_{1m})}$, where $\mathbf{x}_i = (t_i, y_i)^{\mathrm{T}}$). Once the initial condition (t_i^*, E, y_i^*) for the periodic motion is obtained, the switching times and velocities for all the switching planes are determined accordingly. The stability and bifurcation for period-1 motion can be determined through the corresponding Jacobian matrix of the Poincaré

mapping. From Eq. (26), the Jacobian matrix is computed by the chain rule, i.e.,

$$\begin{aligned} DP &= DP_{4(36)^{k_{2n}}32(15)^{k_{1n}}1\cdots 4(36)^{k_{21}}32(15)^{k_{11}}1} = \prod_{i=1}^{n}(DP_4\cdot DP_{36}^{k_{2i}}\cdot DP_3\cdot DP_2\cdot DP_{15}^{k_{1i}}\cdot DP_1) \\ &= \prod_{i=1}^{n}\left(DP_4\cdot\prod_{i_{2i}=1}^{k_{2i}}(DP_3\cdot DP_6)\cdot DP_3\cdot DP_2\cdot\prod_{i_{1i}=1}^{k_{1i}}(DP_1\cdot DP_5)\cdot DP_1\right) \\ &= \underbrace{DP_4\cdot\underbrace{DP_3\cdot DP_6\cdot\cdots\cdot DP_3\cdot DP_6}_{k_{2n}\text{-set(local)}}\cdot DP_3\cdot DP_2\cdot\underbrace{DP_1\cdot DP_5\cdot\cdots\cdot DP_1\cdot DP_5}_{k_{1n}\text{-set(local)}}\cdot DP_1}_{n\text{-global}} \\ &\quad\cdot\cdots\cdot\underbrace{DP_4\cdot\underbrace{DP_3\cdot DP_6\cdot\cdots\cdot DP_3\cdot DP_6}_{k_{21}\text{-set(local)}}\cdot DP_3\cdot DP_2\cdot\underbrace{DP_1\cdot DP_5\cdot\cdots\cdot P_1\cdot P_5}_{k_{11}\text{-set(local)}}\cdot P_1}_{\text{first-global}}. \end{aligned} \tag{27}$$

From mappings in Section 2, two unknowns (t_{i+1}, y_{i+1}) can be expressed through the initial conditions, i.e., $t_{i+1} = t_{i+1}(t_i, y_i)$ and $y_{i+1} = y_{i+1}(t_i, y_i)$. The linearization of mappings P_1 and P_3 in the neighborhood of the solution of periodic motion (t_i^*, y_i^*) generates the Jacobian matrices:

$$\begin{aligned} DP_j &= \left[\frac{\partial(t_{i+1}, y_{i+1})}{\partial(t_i, y_i)}\right]_{(t_i^*, y_i^*, t_{i+1}^*, y_{i+1}^*)} \\ &= \frac{e^{-d(t_{i+1}-t_i)}}{y_{i+1}\omega}\begin{bmatrix} y_i\omega\cos\omega(t_{i+1}-t_i) + N_i\sin\omega(t_{i+1}-t_i) & -\sin\omega(t_{i+1}-t_i) \\ \omega(y_iN_{i+1} - y_{i+1}N_i)\cos\omega(t_{i+1}-t_i) & \omega y_{i+1}\cos\omega(t_{i+1}-t_i) \\ \quad +(N_{i+1}N_i + \omega^2 y_i y_{i+1})\sin\omega(t_{i+1}-t_i) & -N_{i+1}\sin\omega(t_{i+1}-t_i) \end{bmatrix}_{(t_i^*, y_i^*, t_{i+1}^*, y_{i+1}^*)} \end{aligned} \tag{28}$$

The linearization of mappings P_2, P_4, P_5 and P_6 in the neighborhood of (t_i^*, y_i^*) generates the Jacobian matrices for

$$\begin{aligned} DP_j &= \left[\frac{\partial(t_{i+1}, y_{i+1})}{\partial(t_i, y_i)}\right]_{(t_i^*, y_i^*, t_{i+1}^*, y_{i+1}^*)} \\ &= \frac{e^{-2d(t_{i+1}-t_i)}}{2y_{i+1}d} \\ &\quad\times\begin{bmatrix} 2dy_i + a\cos\Omega t_i(e^{2d(t_{i+1}-t_i)} - 1) & 1 - e^{2d(t_{i+1}-t_i)} \\ e^{2d(t_{i+1}-t_i)}P_{i+1}a\cos\Omega t_{i+1} - P_i a\cos\Omega t_{i+1} & a\cos\Omega t_{i+1} - P_{i+1}e^{2d(t_{i+1}-t_i)} \end{bmatrix}_{(t_i^*, y_i^*, t_{i+1}^*, y_{i+1}^*)}, \end{aligned} \tag{29}$$

where

$$N_i = a\cos(\Omega t_i) - dy_i \quad \text{and} \quad P_i = a\cos(\Omega t_i) - 2dy_i. \tag{30}$$

The eigenvalues of a fixed point for the periodic motion mapping is expressed through the trace (Tr(DP)) and determinant (Det(DP)) of the Jacobian matrix DP, i.e.,

$$\lambda_{1,2} = \frac{\mathrm{Tr}(DP)}{2} \pm \frac{\sqrt{[\mathrm{Tr}(DP)]^2 - 4\mathrm{Det}(DP)}}{2}. \tag{31}$$

If $[\mathrm{Tr}(DP)]^2 < 4\mathrm{Det}(DP)$, Eq. (31) is expressed by

$$\lambda_{1,2} = \mathrm{Re}(\lambda) \pm \mathrm{j}\,\mathrm{Im}(\lambda), \quad \text{with } \mathrm{j} = \sqrt{-1}, \tag{32}$$

where $\mathrm{Re}(\lambda) = \mathrm{Tr}(DP)/2$, and $\mathrm{Im}(\lambda) = \sqrt{4\mathrm{Det}(DP) - [\mathrm{Tr}(DP)]^2}/2$.

If two eigenvalues lie inside the unit circle, then the period-1 motion pertaining to the fixed point of the Poincaré mapping is stable, while if one of them lies outside the unit circle, the periodic motion is unstable. Namely, the stable periodic motion requires the eigenvalues to be

$$|\lambda_i| < 1, \quad i = 1, 2. \tag{33}$$

When this condition is not satisfied, the periodic motion is unstable. For complex eigenvalues $|\lambda_{1,2}| < 1$, the periodic motion is a stable focus, while for $|\lambda_{1,2}| > 1$ the periodic motion becomes an unstable focus. If $|\lambda_{1 \text{ or } 2}| = 1$ with complex numbers, namely,

$$\mathrm{Det}(DP) = 1, \tag{34}$$

the Neimark bifurcation occurs. For two eigenvalues being real, the stable-node periodic motion requires $\max|\lambda_i| < 1$, $i = 1, 2$ and the unstable node (or saddle) one requires $|\lambda_i| > 1$, $i = 1$ or 2. The saddle-node of the first kind is as $\lambda_i > 1$, $i = 1$ or 2, and the saddle-node of the second kind needs $\lambda_i < -1$, $i = 1$ or 2. If one of the two eigenvalues is -1 (i.e., $\lambda_{1(\text{or } 2)} = -1$) and the other one is inside the unit cycle, the period-doubling bifurcation occurs. Further, the period-doubling bifurcation condition is

$$\mathrm{Tr}(DP) + \mathrm{Det}(DP) + 1 = 0. \tag{35}$$

If one of the two eigenvalues is $+1$ (i.e., $\lambda_{1(\text{or } 2)} = +1$) and the second one is inside the unit cycle, the first saddle-node bifurcation occurs. Similarly, the corresponding bifurcation condition is

$$\mathrm{Det}(DP) + 1 = \mathrm{Tr}(DP). \tag{36}$$

For the grazing of periodic motion, one of the eigenvalues becomes infinity since the Jacobian matrix is singular.

5. Illustrations

From mapping structures of periodic motions, the switching sets for a specific regular motion can be determined through solving a set of nonlinear equations. For instance, for a periodic motion with a mapping structure $P_{4(36)^{k_{2n}}32(15)^{k_{1n}}1\cdots4(36)^{k_{21}}32(15)^{k_{11}}1}$ (i.e., $P_{4(36)^{k_{2n}}32(15)^{k_{1n}}1\cdots4(36)^{k_{21}}32(15)^{k_{11}}1}\mathbf{x} = \mathbf{x}$), a set of vector equations is as

$$\begin{aligned}
&\mathbf{f}^{(1)}(\mathbf{x}_{i+1}, \mathbf{x}_i) = 0,\\
&\mathbf{f}^{(5)}(\mathbf{x}_{i+2}, \mathbf{x}_{i+1}) = 0,\\
&\vdots\\
&\mathbf{f}^{(4)}\left(\mathbf{x}_{i+4n+2\sum_{m=1}^{n}(k_{1m}+k_{2m})}, \mathbf{x}_{i+4n+2\sum_{m=1}^{n}(k_{1m}+k_{2m})-1}\right) = 0,
\end{aligned} \tag{37}$$

where $\mathbf{f}^{(n_j)} = (f_1^{(n_j)}, f_2^{(n_j)})^{\mathrm{T}}$ is relative to the governing equations of mapping P_{n_j} ($n_i \in \{1, 2, \ldots, 6\}$) and $\mathbf{x}_i = (t_i, \dot{x}_i)^{\mathrm{T}} \equiv (t_i, y_i)^{\mathrm{T}}$. For the period-1 motion per N-periods, the periodicity condition requires

$$\mathbf{x}_{i+4n+2\sum_{m=1}^{n}(k_{1m}+k_{2m})} = \mathbf{x}_i \quad \text{or} \quad \left(t_{i+4n+2\sum_{m=1}^{n}(k_{1m}+k_{2m})}, y_{i+4n+2\sum_{m=1}^{n}(k_{1m}+k_{2m})}\right)^{\mathrm{T}} \equiv \left(t_i + \frac{2N\pi}{\Omega}, y_i\right)^{\mathrm{T}}. \tag{38}$$

Solving Eqs. (37) and (38) generates the switching sets for periodic motion.

Since the spring constant is zero in Region II, the local periodic motion near the switching planes cannot be obtained. Therefore, consider a periodic motion relative to mapping P_{4321} first and a set of system parameters ($d = 0.5, c = 100, E = 1.0, a = 20, N = 1$) is used, and these system parameters will be used for all numerical illustrations. The switching phases and velocities varying with excitation frequency are illustrated in Fig. 8. The circular symbols denote bifurcation points. The thin and thick solid curves represent the stable symmetrical and asymmetric motions, respectively. The dashed and dash–dot curves denote the unstable symmetrical and asymmetrical motions. The switching phases and velocities for the entire range of excitation frequency are plotted in Figs. 8(a) and (b). The complicated parts of the solutions for switching phases and velocities are zoomed in Figs. 8(c) and (d). The local stability conditions are determined through the eigenvalues of the Jocabian matrix in Eq. (27), as shown in Fig. 9. The disappearance grazing of the symmetric motion occurs at $\Omega_{\mathrm{cr1}(s)} \approx 7.39$ and $\Omega_{\mathrm{cr4}(s)} \approx 0.23$. In the range of $\Omega \in (3.38, 7.34)$, the solution of symmetric period-1 motion is stable. For $\Omega \in (7.34, 7.39)$ and $\Omega \in (0.23, 3.38)$, the symmetrical period-1 motion is unstable. At $\Omega_{\mathrm{cr2}(s)} \approx 7.34$ and $\Omega_{\mathrm{cr3}(s)} \approx 3.38$, the saddle bifurcation of the first kind occurs for the symmetrical period-1 motion. In the range of $\Omega \in (0.23, 3.30)$, two asymmetrical period-1 motions exist. At $\Omega_{\mathrm{cr1}(a)} \approx 3.30$, the solutions for symmetrical and asymmetrical motions merge together. The stable, asymmetrical motion is in $\Omega \in (2.98, 3.22)$. The unstable solutions for the two asymmetrical period-1 motions are in $\Omega \in (0.24, 2.98)$ and $\Omega \in (3.22, 3.30)$. At $\Omega_{\mathrm{cr2}(a)} \approx 3.234$, the saddle-node bifurcation of the first kind occurs when the asymmetrical period-1 motion takes place. Furthermore, the period-doubling bifurcation of the asymmetrical period-1 motion occurs at excitation frequency $\Omega_{\mathrm{cr3}(a)} \approx 2.98$. Note that subscripts "a" and "s" denote the *a*symmetrical and *s*ymmetrical motions.

During grazing of the two asymmetric motions of P_{4321}, the motion with the symmetrical mapping structures switches into the right- and left-asymmetrical motions related to mappings $P_{432(15)1}$ and $P_{4(36)321}$, respectively. The mapping structures are qualitatively described in Fig. 5. The switching phases and velocities varying with excitation frequency for the two motions are plotted with parameters ($d = 0.5, c = 100, E = 1.0, a = 20, N = 1$), as shown in Fig. 10. The circular symbols denote bifurcation points. The thin and thick solid curves represent the stable motions for mappings $P_{432(15)1}$ and $P_{4(36)321}$, respectively. The dashed and dash–dot curves denote the corresponding, unstable motions. The stability conditions are presented through the eigenvalue analysis, as illustrated in Fig. 11. For the two motions, one of the two eigenvalues approaches infinity at $\Omega_{\mathrm{cr1}} \approx 2.863$ and $\Omega_{\mathrm{cr4}} \approx 1.529$. It indicates that no motion relative to the two mappings exists for $\Omega < \Omega_{\mathrm{cr4}}$ and $\Omega > \Omega_{\mathrm{cr1}}$. The disappearance grazing of the two motions occurs at $\Omega_{\mathrm{cr1}} \approx 2.863$ and $\Omega_{\mathrm{cr4}} \approx 2.863$. At $\Omega_{\mathrm{cr2}} \approx 2.858$, the saddle-node bifurcation of the first kind occurs. For excitation frequency $\Omega \in (2.858, 2.863)$, the unstable motion is the saddle node of

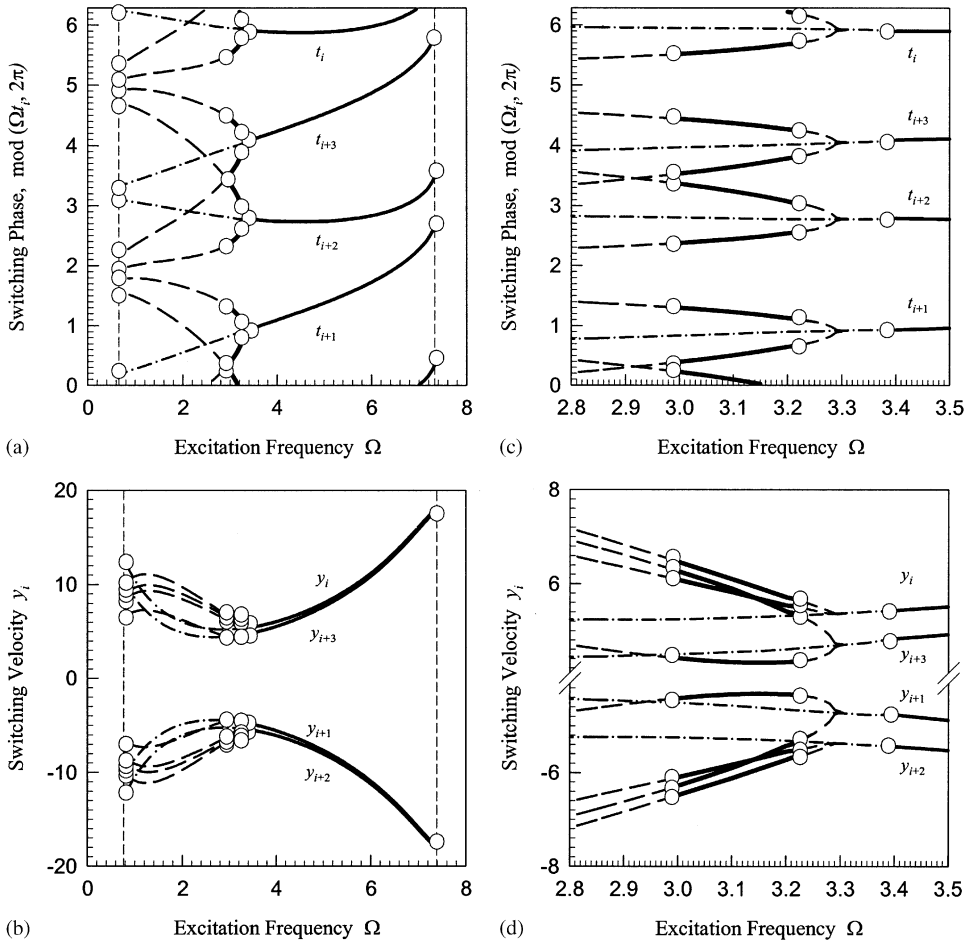

Fig. 8. Switching phases and velocities varying with excitation frequency for periodic motion pertaining to mapping P_{4321}: (a) switching phases and (b) switching velocities; (c) zoomed switching phases and (d) zoomed switching velocities. The circular symbols denote bifurcation points; $d = 0.5$, $c = 100$, $E = 1.0$, $a = 200$; ———, stable symmetric; ▬▬, stable asymmetric; – – –, unstable symmetric; – · – · –, unstable asymmetric.

the first kind, and the stable motion is in $\Omega \in (2.766, 2.858)$. At $\Omega_{cr3} \approx 2.766$, the period-doubling bifurcation (or the saddle node of the second kind) happens. For an excitation frequency near the period-doubling bifurcation point ($\Omega < \Omega_{cr3}$), motions of mapping $P_{432(15)1} \circ P_{432(15)1}$ and $P_{4(36)321} \circ P_{4(36)321}$ can be obtained. The unstable motions of mappings $P_{432(15)1}$ and $P_{4(36)321}$ are the saddle nodes of the second kind in the range $\Omega \in (1.592, 2.766)$. Once the gazing of $P_{432(15)1}$ and $P_{4(36)321}$ takes place, the motion of $P_{4(36)32(15)1}$ appears, as described qualitatively in Fig. 6. The mapping structure for this motion is symmetrical. Thus, the symmetrical and asymmetrical motions for such a mapping structure exist.

The switching phases and velocities of the motion of $P_{4(36)32(15)1}$ for the entire range of excitation frequency are plotted in Fig. 12. The lines and symbols have meanings similar to the

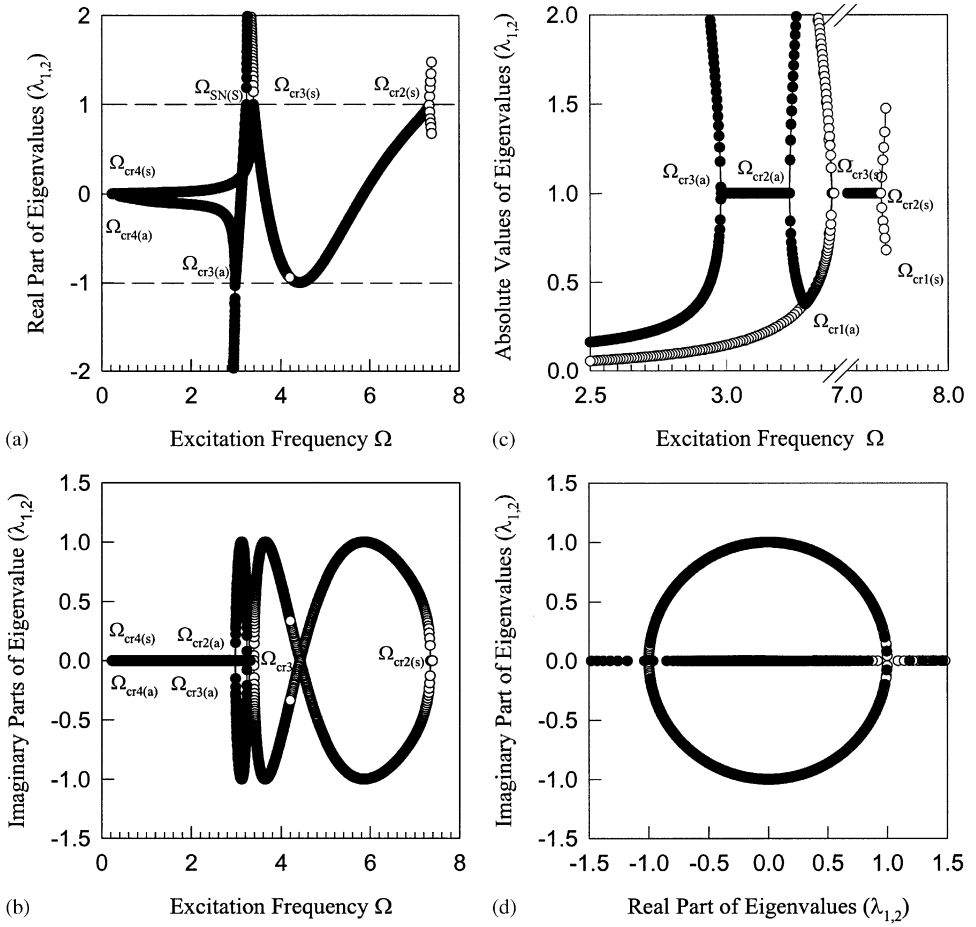

Fig. 9. Eigenvalues for periodic motion relative to mapping P_{4321}: (a) real parts and (b) imaginary parts; (c) absolute values and (d) complex plane. The hollow and solid circular symbols denote symmetrical and asymmetrical periodic motions; $d = 0.5,\ c = 100,\ E = 1.0,\ a = 200$.

ones in Fig. 8. The corresponding eigenvalue analysis for the motions are presented in Fig. 13 for local stability and bifurcation conditions. The solution structure for this motion is similar to the motion of P_{4321}. For the symmetrical motion of $P_{4(36)32(15)1}$, the critical values for disappearance gazing are $\Omega_{cr1(s)} \approx 1.889$ and $\Omega_{cr4(s)} \approx 0.176$. The saddle-node bifurcation points of the first kind are $\Omega_{cr2(s)} \approx 1.88$ and $\Omega_{cr3(s)} \approx 1.706$. For the asymmetrical motion of $P_{4(36)32(15)1}$, the critical values for the disappearance grazing are $\Omega_{cr1(a)} \approx 1.65$ and $\Omega_{cr4(a)} \approx 0.788$, and the saddle-node bifurcation points of the first and second kinds are $\Omega_{cr2(a)} \approx 1.614$ and $\Omega_{cr3(a)} \approx 1.592$, respectively.

To demonstrate how to determine motions relative to a complicated mapping structure, the motion of mapping $P_{4(36)^2 32(15)^2 1}$ is presented in Fig. 14 with the same parameter as above. The lines and symbols have meanings similar to the ones in Fig. 8. Similarly, for the symmetrical

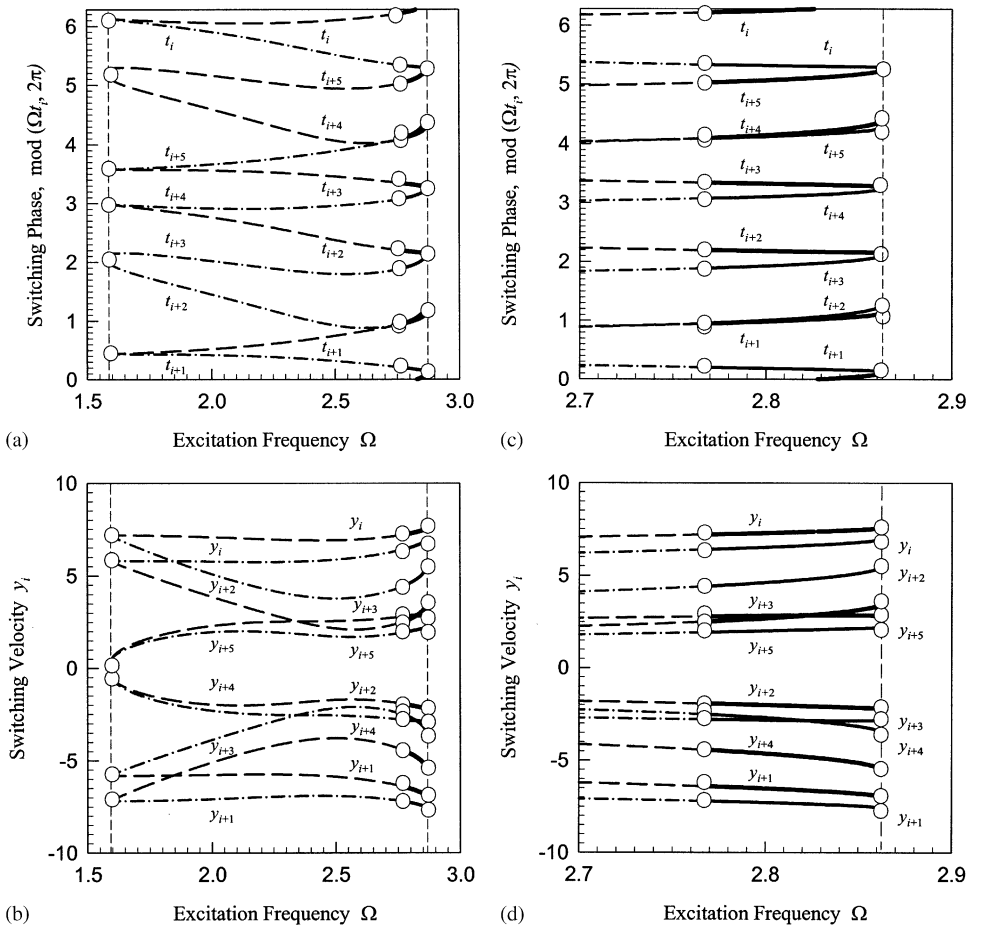

Fig. 10. Switching phases and velocities varying with excitation frequency for periodic motions pertaining to mapping $P_{4(36)321}$ and $P_{432(15)1}$: (a) switching phases and (b) switching velocities; (c) zoomed switching phases and (d) zoomed switching velocities. The circular symbols denote bifurcation points; $d = 0.5$, $c = 100$, $E = 1.0$, $a = 200$; ———, stable $P_{432(15)1}$; ▬▬, stable $P_{4(36)321}$; – – –, unstable $P_{4(36)321}$; – · – · –, unstable $P_{432(15)1}$.

motion of $P_{4(36)^2 32(15)^2 1}$, the critical values for disappearance gazing are $\Omega_{\mathrm{cr1}(s)} \approx 1.231$ and $\Omega_{\mathrm{cr4}(s)} \approx 0.129$. The saddle-node bifurcation points of the first kind are $\Omega_{\mathrm{cr2}(s)} \approx 1.228$ and $\Omega_{\mathrm{cr3}(s)} \approx 1.181$. For the two asymmetrical motions of $P_{4(36)^2 32(15)^2 1}$, the critical values for the disappearance grazing are $\Omega_{\mathrm{cr1}(a)} \approx 1.135$ and $\Omega_{\mathrm{cr4}(a)} \approx 0.753$, and the saddle-node bifurcation points of the first and second kinds are $\Omega_{\mathrm{cr2}(a)} \approx 1.117$ and $\Omega_{\mathrm{cr3}(a)} \approx 1.113$, respectively.

From the above illustrations of periodic motion with mapping $P_{4(36)^m 32(15)^m 1}$, the solutions for the two asymmetric motions have the following relations:

$$
\begin{aligned}
&|\mathrm{mod}(\Omega t^I_{i+j}, 2\pi) - \mathrm{mod}(\Omega t^{II}_{i+\mathrm{mod}(2m+2+j,4m+4)}, 2\pi)| = \pi,\\
&y^I_{i+j} = -y^{II}_{i+\mathrm{mod}(2m+2+j,4m+4)}, \quad \text{for } j = \{0, 1, \ldots, 4m+3\},
\end{aligned} \tag{39}
$$

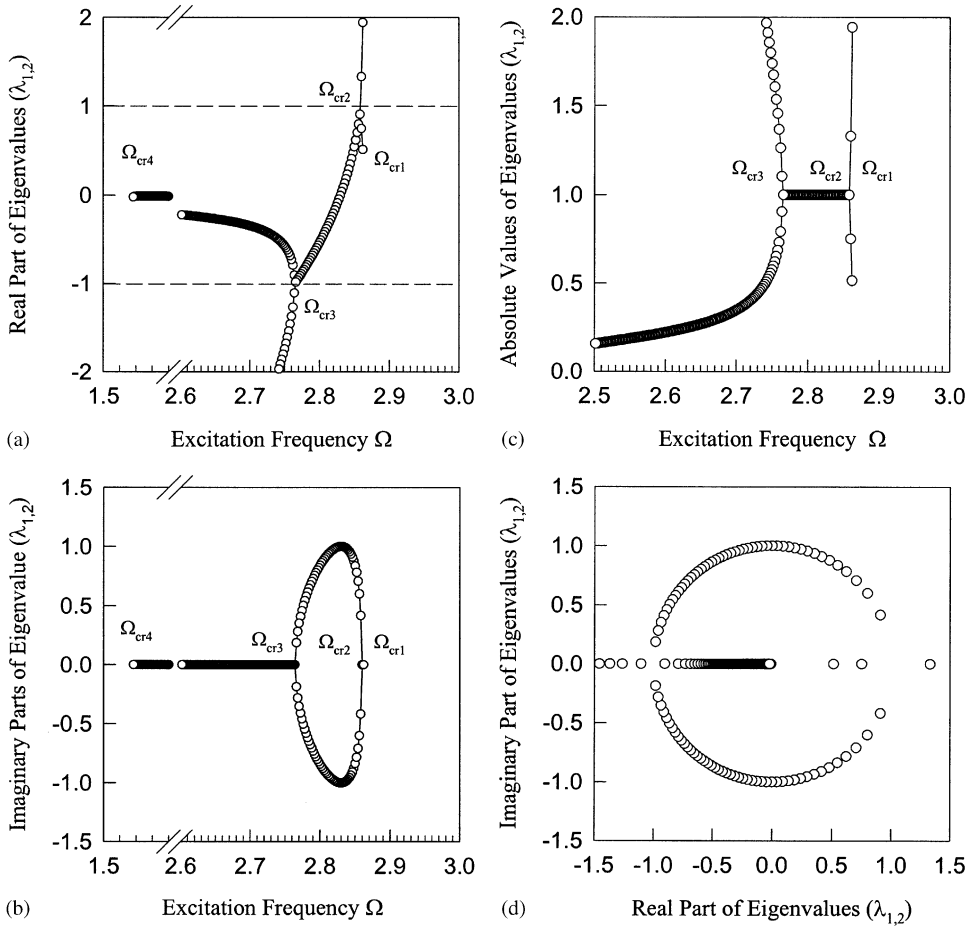

Fig. 11. Eigenvalues for periodic motions relative to mapping $P_{4(36)321}$ and $P_{432(15)1}$: (a) real parts and (b) imaginary parts; (c) absolute values and (d) complex plane. The hollow and solid circular symbols denote symmetrical and asymmetrical periodic motions; $d = 0.5$, $c = 100$, $E = 1.0$, $a = 200$.

where mod(•, •) is the modulus function. For the periodic motion of mapping $P_{4(36)^{m+1}32(15)^m1} = P_I$ and $P_{4(36)^m32(15)^{m+1}1} = P_{II}$, the solution relationship becomes

$$\begin{aligned} &|\mathrm{mod}(\Omega t^I_{i+j}, 2\pi) - \mathrm{mod}(\Omega t^{II}_{i+\mathrm{mod}(2m+4+j,4m+6)}, 2\pi)| = \pi, \\ &y^I_{i+j} = -y^{II}_{i+\mathrm{mod}(2m+4+j,4m+6)}, \quad \text{for } j = \{0, 1, \ldots, 4m+5\}, \end{aligned} \tag{40}$$

or

$$\begin{aligned} &|\mathrm{mod}(\Omega t^{II}_{i+j}, 2\pi) - \mathrm{mod}(\Omega t^I_{i+\mathrm{mod}(2m+2+j,4m+6)}, 2\pi)| = \pi, \\ &y^I_{i+j} = -y^{II}_{i+\mathrm{mod}(2m+2+j,4m+6)}, \quad \text{for } j = \{0, 1, \ldots, 4m+5\}. \end{aligned} \tag{41}$$

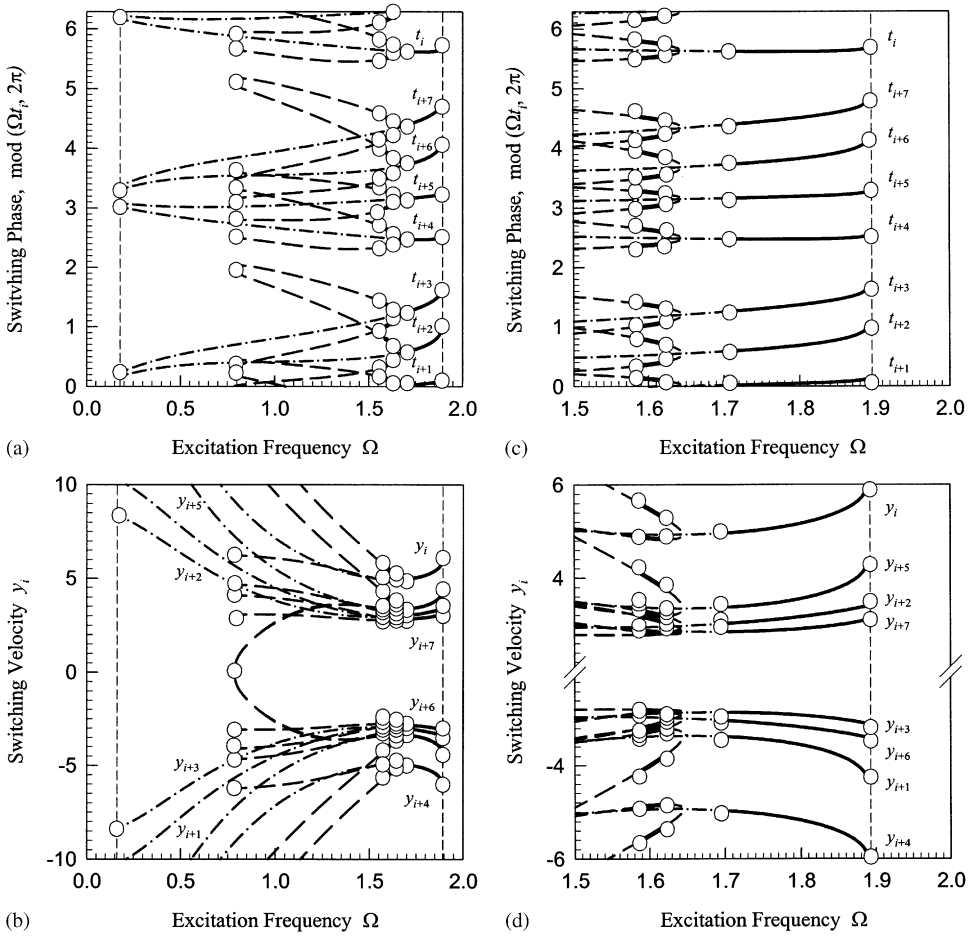

Fig. 12. Switching phases and velocities varying with excitation frequency for periodic motion pertaining to mapping $P_{4(36)32(15)1}$: (a) switching phases and (b) switching velocities; (c) zoomed switching phases and (d) zoomed switching velocities. The circular symbols denote bifurcation points; $d = 0.5$, $c = 100$, $E = 1.0$, $a = 200$; ———, stable symmetric; ▬▬, stable asymmetric; – – –, unstable symmetric; – · – · –, unstable asymmetric.

6. Numerical simulations

From mapping structures, the switching velocity and phases at switching planes are determined. The symmetrical structures of solutions are observed, as summarized in Eqs. (39)–(41). The motions can be simulated numerically through the differential equation (1) with appropriate initial conditions selected from the switching sets determined analytically for this problem, since the analytical expressions of solution for motions in each region are developed. The numerical simulation can be carried out by use of those analytical expressions. Herein, numerical simulations are based on Eqs. (A.2)–(A.6) for the switching planes at $(y_i > 0, x_i = E)$ and $(y_i < 0, x_i = -E)$,

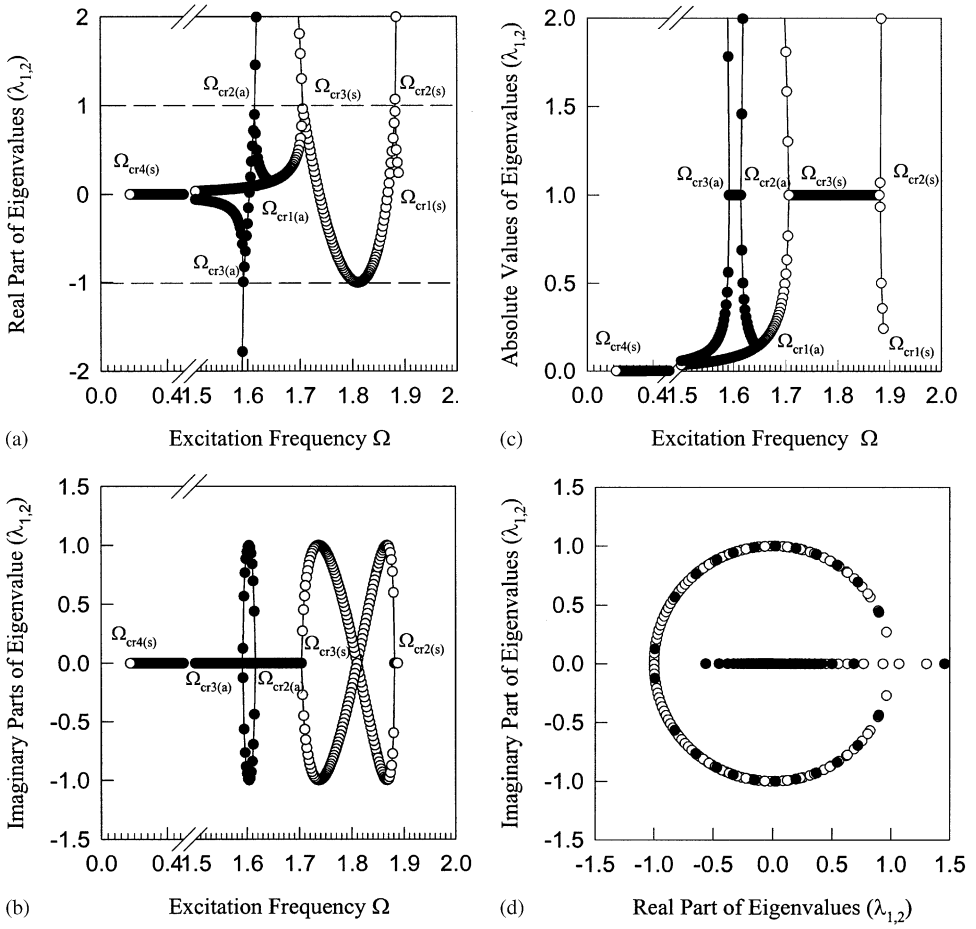

Fig. 13. Eigenvalues for periodic motion relative to mapping $P_{4(36)32(15)1}$: (a) real parts and (b) imaginary parts; (c) absolute values and (d) complex plane. The hollow and solid circular symbols denote symmetrical and asymmetrical periodic motions; $d = 0.5$, $c = 100$, $E = 1.0$, $a = 200$.

and Eqs. (A.8)–(A.12) for $(y_i < 0, x_i = E)$ and $(y_i > 0, x_i = -E)$, respectively. The initial conditions are selected from the switching plane $(t_i, y_i) \in \Sigma_+^+$ given analytically. For comparison, a set of parameters $(A = 10,\ C = 50,\ E = 1,\ D = 0.5,\ M = 0.5)$ is used again. The computation precision at switching planes is 10^{-10}. The input data for all numerical simulations are listed in Table 1.

In Fig. 15, the motion relative to mapping P_{4321} is illustrated. The stable, symmetric, right-asymmetric and left-asymmetric motions are arranged in Figs. 15(a)–(c), respectively. The shape changes of motion in phase planes for such a symmetry are very clearly observed. The phase trajectory in Fig. 15(b) turning 180° clockwise is identical to the phase trajectory in Fig. 15(c). The two asymmetric motions are skew-symmetric, as in Eq. (39). In Figs. 15(d)–(f), the unstable symmetric, right-asymmetric and left-asymmetric motions are presented. Once the symmetric

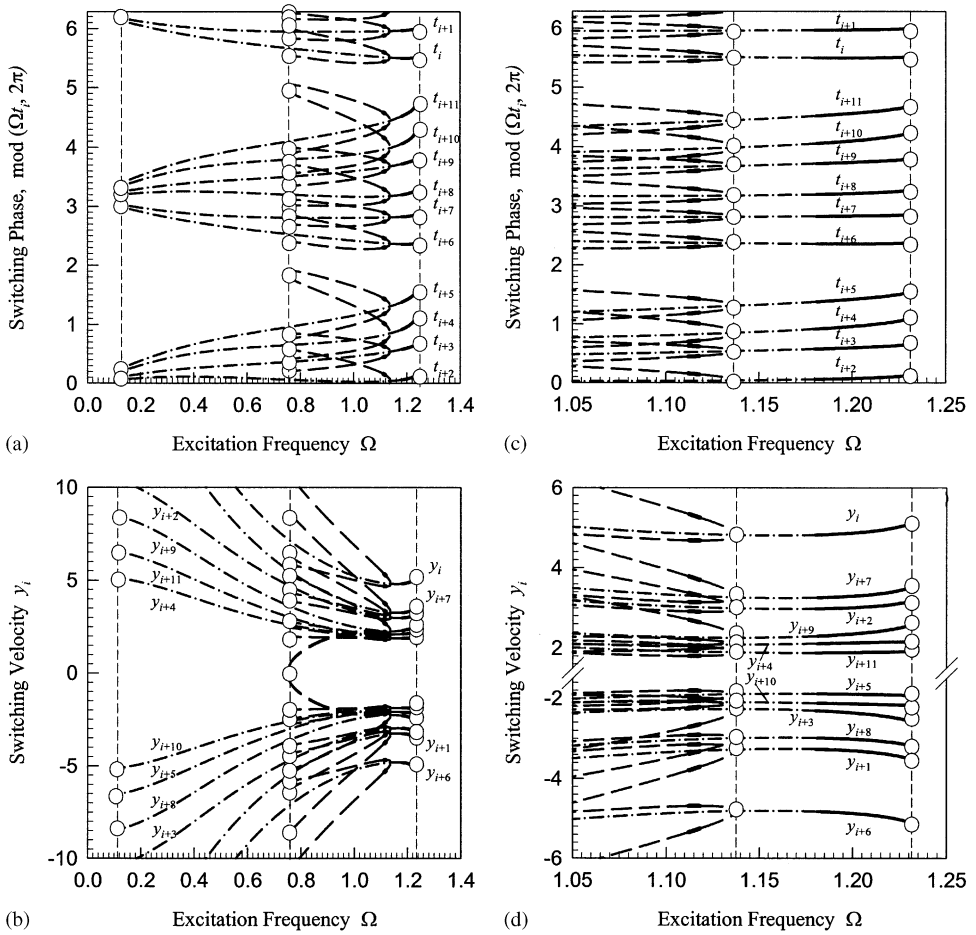

Fig. 14. Switching phases and velocities varying with excitation frequency for periodic motion pertaining to mapping $P_{4(36)^2(32)(15)^21}$: (a) switching phases and (b) switching velocities; (c) zoomed switching phases and (d) zoomed switching velocities. The circular symbols denote bifurcation points; $d = 0.5$, $c = 100$, $E = 1.0$, $a = 200$; ———, stable symmetric; ▬▬, stable asymmetric; – – –, unstable symmetric; – · – · –, unstable asymmetric.

motion loses its stability, the unstable motion may go to one of the closest, other stable motions or chaotic motion, as shown in Fig. 15(d). For the unstable asymmetrical motion, the skew-symmetry property cannot hold any more, which is observed from Figs. 15(e) and (f). The phase trajectories for mappings $P_{432(15)1}$ and $P_{4(36)321}$ are illustrated in Fig. 16. For the stable motions, the trajectories are skew-symmetric. The two solutions have a similar relation as in Eqs. (40) and (41). However, the corresponding unstable motions destroy the skew-symmetry existing in the stable motions. In Fig. 17, the stable, symmetric, right-asymmetric and left-asymmetric motions for $P_{4(36)32(15)1}$ and $P_{4(36)^2 32(15)^2 1}$ are demonstrated in Figs. 17(a)–(c) and (d)–(f), respectively, and the skew-symmetric structures for the asymmetrical motions are observed.

Table 1
Input data for numerical simulations ($d = 0.5, c = 100, E = 1.0, a = 20, x_0 = E, N = 1$)

		Ω	Ωt_0	y_0	Mapping	Symmetry	Stability
Fig. 15	(a)	4.8	5.8782	7.5617		Symmetric	Stable
	(b)	3.2	5.6830	5.5475		R-asymmetric	
	(c)	3.2	6.2195	5.7207	P_{4321}	L-asymmetric	
	(d)	2.5	6.0033	5.3625		Symmetric	Unstable
	(e)	2.5	5.3394	7.4599		R-asymmetric	
	(f)	2.5	5.3502	7.3412		L-asymmetric	
Fig. 16	(a)	2.8	5.3225	4.6288	$P_{432(15)1}$	R-asymmetric	Stable
	(b)	2.8	6.2502	7.2810	$P_{4(36)321}$	L-asymmetric	
	(c)	2.0	5.9064	5.0923	$P_{432(15)1}$	R-asymmetric	Unstable
	(d)	2.0	6.0587	7.0792	$P_{4(36)321}$	L-asymmetric	
Fig. 17	(a)	1.8	5.6161	5.1735		Symmetric	Stable
	(b)	1.6	5.5191	4.8633	$P_{4(36)32(15)1}$	R-asymmetric	
	(c)	1.6	5.7805	5.4937		L-asymmetric	
	(d)	1.2	5.5008	4.8697		Symmetric	
	(e)	1.115	5.6017	5.2969	$P_{4(36)^2 32(15)^2 1}$	R-asymmetric	
	(f)	1.115	5.4467	4.6830		L-asymmetric	

Note that the letters "R" and "L" denote the right and left switching planes. R- (or L-) asymmetric is the asymmetric motion near the right (or left) switching plane.

7. Conclusion

In this paper, the mapping dynamics of periodic motions for a three-piecewise linear system under a periodic excitation is developed, and the mapping structures for all the possible periodic motions are developed. Based on the mapping structures, the analytical prediction of stable and unstable periodic motions is given. No local periodic motion can be obtained since the spring constant in Region II is equal to zero. The symmetry for the stable asymmetrical periodic motions of such a system is observed. The methodology presented in this paper is applicable to other non-smooth systems such as friction-induced vibration, impact oscillator and power control systems.

Appendix A. Basic solutions

For Regions I and III, Eq. (1) becomes a linear equation of the form

$$\ddot{x} + 2d\dot{x} + cx = \pm e + a\cos\Omega t. \tag{A.1}$$

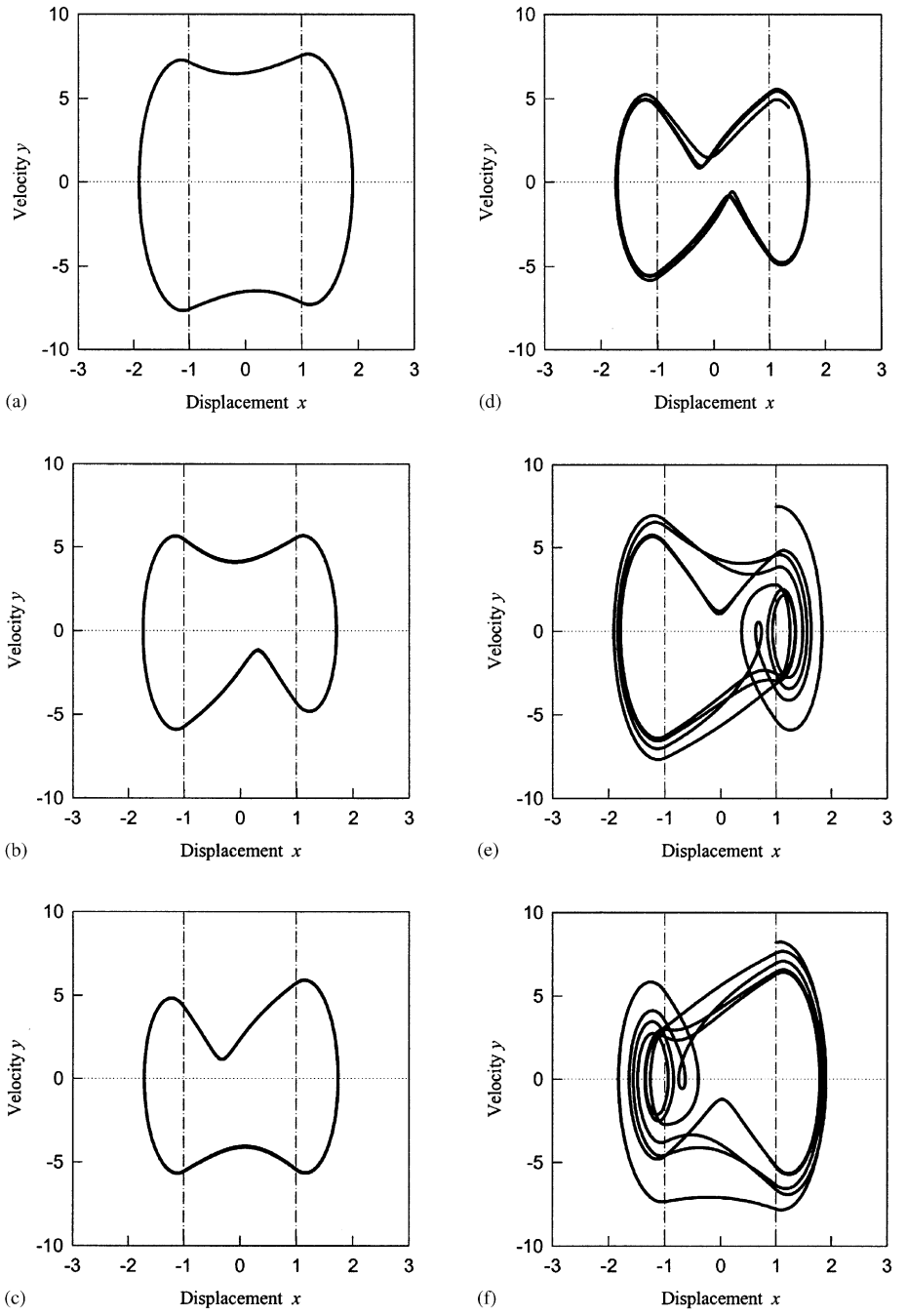

Fig. 15. Phase planes for P_{4321} (a) symmetrical motion, $\Omega = 4.8$, $\Omega t_i \approx 5.8782$, $y_i \approx 7.5617$, (b) asymmetrical motion; $\Omega = 3.2$, $\Omega t_i \approx 5.6830$, $y_i = 5.5475$; (c) asymmetrical motion, $\Omega = 3.2$, $\Omega t_i \approx 6.2195$, $y_i \approx 5.7207$; (d) unstable symmetrical motion, $\Omega = 2.5$, $\Omega t_i \approx 6.0033$, $y_i \approx 5.3625$; (e) unstable asymmetrical motion, $\Omega = 2.5$, $\Omega t_i \approx 5.3394$, $y_i \approx 7.4599$; and (f) unstable asymmetrical motion, $\Omega = 2.5$, $\Omega t_i \approx 5.3502$, $y_i \approx 7.3412$; $d = 0.5$, $c = 100$, $E = 1.0$, $a = 200$.

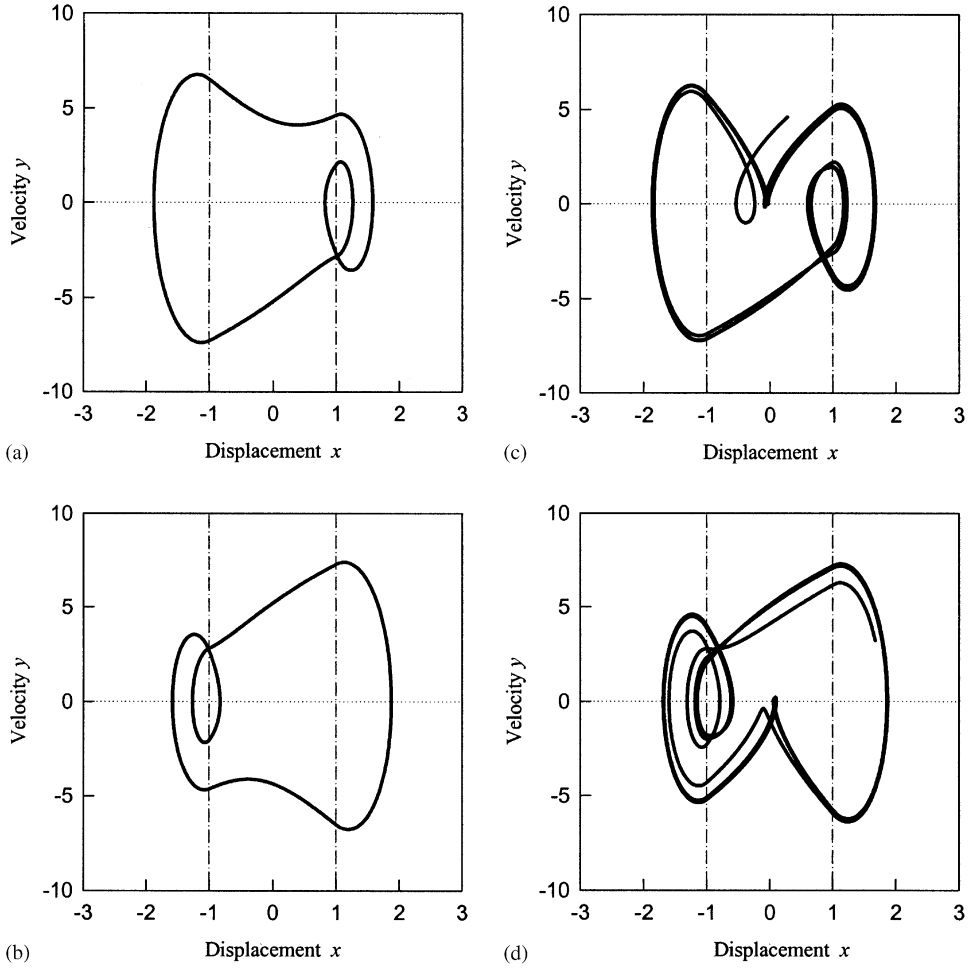

Fig. 16. Phase planes: (a) stable motion for $P_{432(15)1}$, $\Omega = 2.8$, $\Omega t_i \approx 5.3225$, $y_i \approx 4.6288$; (b) stable motion for $P_{4(36)321}$, $\Omega = 2.8$, $\Omega t_i \approx 6.2502$, $y_i \approx 7.2810$; (c) unstable motion relative to $P_{432(15)1}$, $\Omega = 2.0$, $\Omega t_i \approx 5.9064$, $y_i \approx 5.0923$; and (d) unstable motion relative to $P_{4(36)321}$, $\Omega = 2.0$, $\Omega t_i \approx 6.0587$, $y_i \approx 7.0792$; $d = 0.5$, $c = 100$, $E = 1.0$, $a = 200$.

Assuming an initial condition $(t, x, \dot{x}) = (t_i, x_i, y_i)$, the general solution of Eq. (A.1) is given by

$$x(t) = [C_1(t_i)\cos\omega(t - t_i) + C_2(t_i)\sin\omega(t - t_i)]e^{-d(t-t_i)} + x_i + a(D_1\cos\Omega t + D_2\sin\Omega t), \quad (A.2)$$

$$\dot{x}(t) = \{[C_2(t_i)\omega - C_1(t_i)d]\cos\omega(t - t_i) - [C_1(t_i)\omega + C_2(t_i)d]\sin\omega(t - t_i)\}e^{-d(t-t_i)} - a\Omega(D_1\sin\Omega t - D_2\cos\Omega t), \quad (A.3)$$

where two constants $C_1(t_i)$ and $C_2(t_i)$ are determined by the initial condition, i.e.,

$$C_1(t_i) = -a(D_1\sin\Omega t_i + D_2\cos\Omega t_i), \quad (A.4)$$

$$C_2(t_i) = \frac{1}{\omega}\{y_i - a[(D_1\Omega - D_2 d)\sin\Omega t_i + (D_1 d + D_2\Omega)\cos\Omega t_i]\}, \quad (A.5)$$

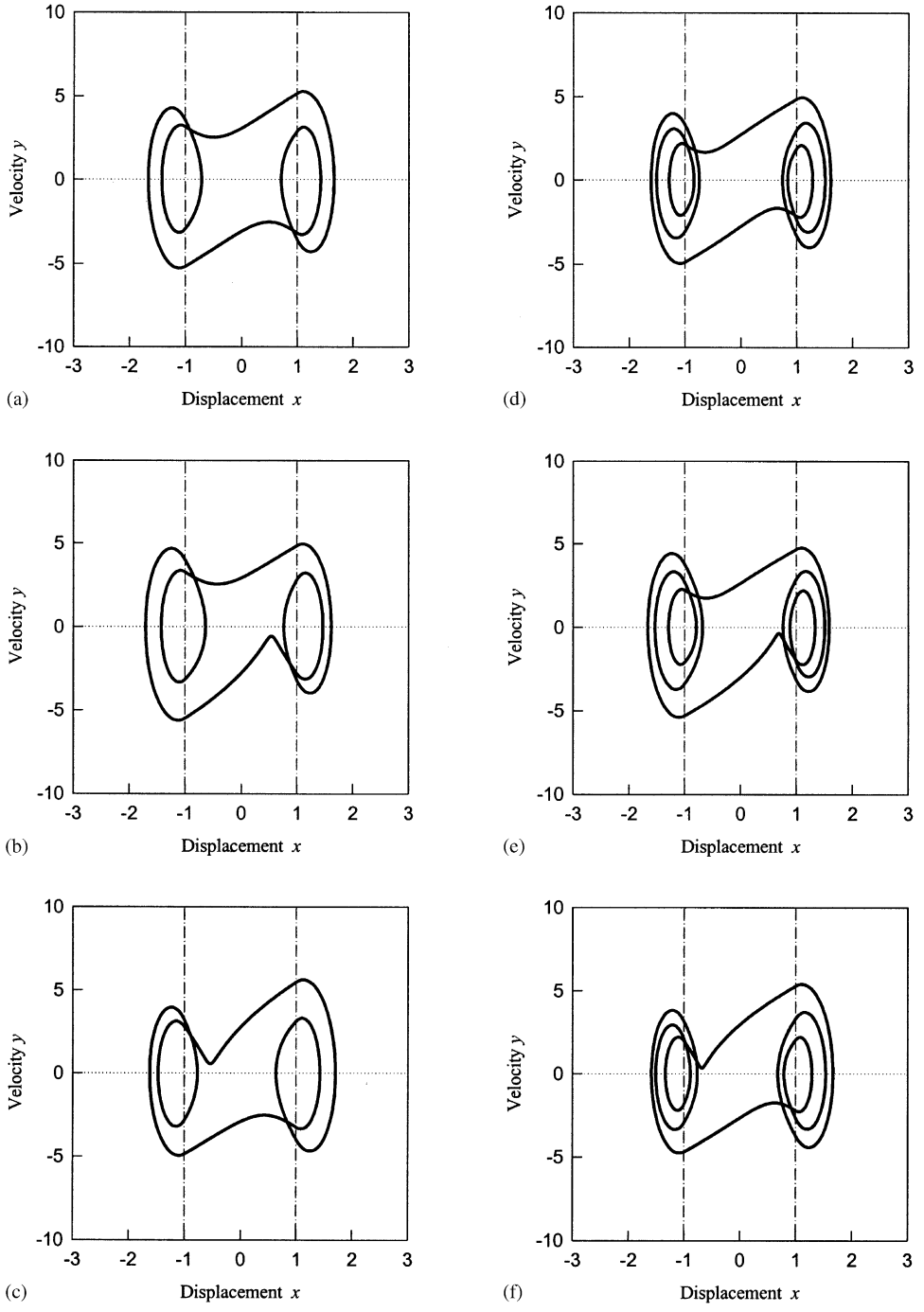

Fig. 17. Phase planes for motions of $P_{4(36)32(15)1}$: (a) symmetric, $\Omega = 1.8$, $\Omega t_i \approx 5.6161$, $y_i \approx 5.1735$; (b) asymmetric, $\Omega = 1.6$, $\Omega t_i \approx 5.5191$, $y_i \approx 4.8633$; (c) asymmetric, $\Omega = 1.6$, $\Omega t_i \approx 5.7805$, $y_i \approx 5.4937$; phase planes for motions of $P_{4(36)^2 32(15)^2 1}$; (d) symmetric, $\Omega = 1.2$, $\Omega t_i \approx 5.5008$, $y_i \approx 4.8697$; (e) asymmetric, $\Omega = 1.115$, $\Omega t_i \approx 5.4467$, $y_i \approx 4.6830$; and (f) asymmetric, $\Omega = 1.115$, $\Omega t_i \approx 5.6017$, $y_i \approx 5.2969$; $d = 0.5$, $c = 100$, $E = 1.0$, $a = 200$.

and

$$x_i = \pm E, \quad \omega = \sqrt{c - d^2}, \quad D_1 = \frac{c - \Omega^2}{(c - \Omega^2)^2 + (2d\Omega)^2}, \quad D_2 = \frac{2d\Omega}{(c - \Omega^2)^2 + (2d\Omega)^2}. \tag{A.6}$$

Note that $x_i = E$ for Region I and $x_i = -E$ for Region III.

For Region II, the form of Eq. (1) reduces to

$$\ddot{x} + 2d\dot{x} = a\cos\Omega t. \tag{A.7}$$

Again, an initial condition $(t, x, \dot{x}) = (t_i, x_i, y_i)$ is assumed and the general solution to Eq. (A.7) is

$$x(t) = C_3(t_i)e^{-2d(t-t_i)} + C_4(t_i) + a(D_3\cos\Omega t + D_4\sin\Omega t), \tag{A.8}$$

$$\dot{x}(t) = -2dC_3(t_i)e^{-2d(t-t_i)} - a\Omega(D_3\sin\Omega t - D_4\cos\Omega t). \tag{A.9}$$

Using the initial condition in Eqs. (A.8) and (A.9) leads to the two new constants $C_3(t_i)$ and $C_4(t_i)$:

$$C_3(t_i) = -\frac{1}{2d}[y_i + a\Omega(D_3\sin\Omega t_i - D_4\cos\Omega t_i)], \tag{A.10}$$

$$C_4(t_i) = \frac{1}{2d}\left(y_i + 2dx_i - \frac{a}{\Omega}\sin\Omega t_i\right), \tag{A.11}$$

and

$$D_3 = \frac{-1}{\Omega^2 + 4d^2}, \quad D_4 = \frac{2d}{\Omega(\Omega^2 + 4d^2)}. \tag{A.12}$$

For starting points at $x = \pm E$, $x_i = \pm E$ accordingly.

References

[1] H. Poincaré, *Les Methods Nouvelles de la Mecanique Celeste*, vol. 1, Gauthier-Villars, Paris, 1892.

[2] C.D. Birkhoff, On the periodic motions of dynamical systems, *Acta Mathematica* 50 (1927) 359–379.

[3] E.A. Corddington, N. Levinson, *Theory of Ordinary Differential Equations*, McGraw-Hill, New York, 1955.

[4] M. Henon, C. Heiles, The applicability of the third integral motion: some numerical experiments, *Astronomical Journal* 69 (1964) 73–79.

[5] Y. Ueda, Steady motion exhibited by Duffing's equation: a picture book of regular and chaotic motion, in: P.J. Holmes (Ed.), *New Approaches to Nonlinear Problems in Dynamics*, SIAM, Philadelphia, 1980, pp. 311–322.

[6] S.W. Shaw, P.J. Holmes, A periodically forced piecewise linear oscillator, *Journal of Sound and Vibration* 90 (1) (1983) 121–155.

[7] A.B. Nordmark, Non-periodic motion caused by grazing incidence in an impact oscillator, *Journal of Sound and Vibration* 145 (1991) 279–297.

[8] M. Kleczka, E. Kreuzer, W. Schiehlen, Local and global stability of a piecewise linear oscillator, *Philosophical Transactions of the Royal Society of London: Physical Sciences and Engineering, Nonlinear Dynamics of Engineering Systems* 338 (1992) 533–546.

[9] S. Foale, Analytical determination of bifurcations in an impact oscillators, *Philosophical Transactions of the Royal Society of London* 347 (1994) 353–364.

[10] A.C.J. Luo, Analytical Modeling of Bifurcations, Chaos and Multifactals in Nonlinear Dynamics, Ph.D. Dissertation, University of Manitoba, Manitoba, Canada, 1995.

[11] R.P.S. Han, A.C.J. Luo, W. Deng, Chaotic motion of a horizontal impact pair, *Journal of Sound and Vibration* 181 (1995) 231–250.
[12] A.C.J. Luo, R.P.S. Han, Dynamics of a bouncing ball with a periodic vibrating table revisited, *Nonlinear Dynamics* 10 (1996) 1–18.
[13] A.C.J. Luo, An unsymmetrical motion in a horizontal impact oscillator, *Journal of Vibrations and Acoustics* 124 (2002) 420–426.
[14] G.X. Li, R.H. Rand, F.C. Moon, Bifurcation and chaos in a forced zero-stiffness impact oscillator, *International Journal of Nonlinear Mechanics* 25 (4) (1990) 414–432.
[15] S. Menon, A.C.J. Luo, An analytical prediction of the global period-1 motion in a periodically forced, piecewise linear system, *International Journal of Bifurcation and Chaos*, in press.
[16] J.P.D. Hartog, S.J. Mikina, Forced vibrations with non-linear spring constants, *Journal of Applied Mechanics* 58 (1932) 157–164.
[17] S. Timoshenko, *Vibration Problems in Engineering*, Van Nostrand, New York, 1937.
[18] S. Natsiavas, Periodic response and stability of oscillators with symmetric trilinear restoring force, *Journal of Sound and Vibration* 134 (2) (1989) 315–331.
[19] S. Natsiavas, G. Verros, Dynamics of oscillators with strongly nonlinear asymmetric damping, *Nonlinear Dynamics* 20 (1999) 221–246.
[20] S. Theodossiades, S. Natsiavas, Non-linear dynamics of gear-pair systems with periodic stiffness and backlash, *Journal of Sound and Vibration* 229 (2) (2000) 287–310.